

# CMA-Net: A Cascaded Mutual Attention Network for Light Field Salient Object Detection

Yi Zhang

Lu Zhang

Wassim Hamidouche

Olivier Deforges

**Abstract**—In the past few years, numerous deep learning methods have been proposed to address the task of segmenting salient objects from RGB images. However, these approaches depending on single modality fail to achieve the state-of-the-art performance on widely used light field salient object detection (SOD) datasets, which collect large-scale natural images and provide multiple modalities such as multi-view, micro-lens images and depth maps. Most recently proposed light field SOD methods have improved detecting accuracy, yet still predict rough objects’ structures and perform slow inference speed. To this end, we propose *CMA-Net*, which consists of two novel cascaded mutual attention modules aiming at fusing the high level features from the modalities of all-in-focus and depth. Our proposed *CMA-Net* outperforms 30 state-of-the-art SOD methods on two widely applied light field benchmark datasets. Besides, the proposed *CMA-Net* is able to inference at the speed of 53 fps. Extensive quantitative and qualitative experiments illustrate both the effectiveness and efficiency of our *CMA-Net*, inspiring future development of multi-modal learning for both the RGB-D and light field SOD.

**Index Terms**—light field, multi-modal, salient object detection, mutual attention, RGB-D.

## I. INTRODUCTION

Learning to segment the salient objects that grasp most of the human visual attention from given images is of great importance for various computer vision applications such as video object segmentation [1] and image caption generation [2]. In the past years, hundreds of deep learning methods have been proposed to address salient object detection (SOD) in RGB images [3]. However, models based on single modality hardly reflect the real human visual mechanism which depends on inputs of multiple modalities (e.g., multi-view images, micro-lens images and depth information), also fail to achieve top performance on challenging multi-modal SOD benchmarks [4].

As the development of light field cameras (e.g. Lytro), it is feasible to collect large-scale natural images in various modalities such as multi-view images, micro-lens images, focal stacks and depth maps [5]. These multi-modal light field data provide rich information to approximate the genuine representation of how light exists in the real world. Recently, SOD on light field appeals increasing attention from the computer vision community, which is attributed to the establishment of light field SOD benchmark datasets including LFSD [5], HFUT [6], DUT-LF [7] and DUT-MV [8]. To the best of our knowledge, focal stack-based solutions, i.e., ERNet-teacher (ERNetT) [9] and MoLF [4] are the state-of-the-arts on so far the largest light field SOD benchmark [9], with the training sets of about 1K all-in-focus (AiF) images (also known as RGB images in

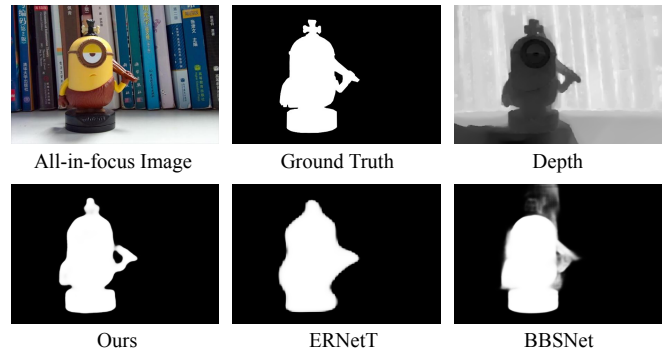


Fig. 1. An example of SOD with our *CMA-Net* and the state-of-the-art multi-modal methods, i.e., ERNetT [9] and BBSNet [10].

mono-modal SOD). However, as show in Fig. 1, current state-of-the-art RGB-D methods (e.g., BBSNet [10]) or light field approaches (e.g., ERNetT [9]) fail challenging cases by giving poor prediction of salient objects’ structures, owing to the inefficiency of traditional attention mechanisms used for multi-modal fusion (details in § II-B). Besides, due to the spatial complexity of focal stacks (e.g., a focal stack usually consists of 12 natural images with focuses on multiple depths [4]) corresponding to each of the AiF images, existing top-ranked light field methods (e.g., ERNetT owns an inference speed of 14 fps) are hardly applied to on-line SOD applications.

To this end, we propose a novel mutual attention mechanism established between the modalities of AiF images and depth maps (Fig. 1). We further construct a cascaded mutual attention network (*CMA-Net*) to synchronously fuse and decode the high-level features from the two modalities. Our proposed *CMA-Net* outperforms 30 SOD methods, also with a relatively high running speed (53 fps). In a nutshell, we provide four main contributions as follows:

- We propose a new mutual attention mechanism to efficiently fuse the multi-modal high level features. Note that the proposed attention mechanism can be used as a basic module and embedded to different networks.
- We further build *CMA-Net* which consists of two cascaded novel attention modules, to conduct SOD with the inputs of only two modalities, i.e., AiF images and depth maps. Our *CMA-Net* does not apply focal stacks, also avoids processing low-level features from both the modalities, thus performing competitive inference speed.
- We conduct systematical benchmark experiments involv-

ing 30 baselines, four metrics and two widely used light field datasets, to illustrate the superiority of our *CMA-Net*.

- We present thorough ablation studies to prove the effectiveness of proposed attention mechanism and the necessity of depth information for conducting light field SOD.

## II. RELATED WORKS

In this section, we briefly introduce recent works from the aspects of light field SOD datasets, methods, and attention mechanisms used for cross modal fusion.

### A. Light Field SOD

1) *Methods*: To the best of our knowledge, the existing methods include 10 traditional ones ([5], [6], [11]–[18]) and 7 deep learning-based ones ([4], [7]–[9], [19]–[21]), respectively. Traditional methods such as DILF [18], BIF [13], MA [6], SGDC [15] and DCA [17] used depth maps as auxiliary inputs, and took advantage of handcrafted features such as color contrast and objects’ location cues towards multi-modal SOD. Methods such as ERNetT [9] and MoLF [4] applied stacked natural images in various depths, thus achieving good performances on light field benchmarks. However, these methods tend to be slow during testing, due to the high computational cost induced by the inputs consisting of focal stacks.

### B. Attention for Cross Modal Fusion

In the field of multi-modal SOD, several cross modal attention mechanisms have been recently proposed. S2MA [22] designed a self-mutual attention module to automatically select useful high-level features learned from both modalities. BBSNet [10] constructed depth-enhanced module to combine the channel and spatial attention at each of the encoding stages. DLLF [7], LFNNet [19], MoLF [4] and ERNetT [9] all employed classical channel attention [23] to aid the feature selection and refinement from the modality of focal stacks. Recent large-scale light field SOD benchmark studies (e.g., [4], [9]) indicate that it remains an open question how to efficiently fuse the intrinsic features from multiple modalities for advanced detecting accuracy.

## III. CASCADED MUTUAL ATTENTION NETWORK

The *CMA-Net* consists of a duel-branch ResNet50 [24]-based encoder and a cascaded mutual attention-based decoder.

### A. RGB-D Encoder

Our encoder is a duel-branch architecture that consists of symmetrical convolutional layers transferred from ImageNet-pretrained ResNet50 [24]. In *CMA-Net*, we only process the high-level features, i.e., the features ( $\{f_i^{\text{AiF}}\}_{i=2}^4$  and  $\{f_i^{\text{Dep}}\}_{i=2}^4$ ) from the last three layers of ResNets, to focus on salient objects’ shape and location cues [25] also to avoid extra computational cost. The  $\{f_i^{\text{AiF}}\}_{i=2}^4$  and  $\{f_i^{\text{Dep}}\}_{i=2}^4$  are then fed into a series of receptive field blocks [25] to enrich the global context information from each encoding level (Fig. 2).

### B. Cascaded Mutual Attention

1) *Multi-level Concatenation*: The refined high level features from adjacent encoding stages, e.g.,  $f_{\text{RFB}}^{\text{AiF}}(i)$  and  $f_{\text{RFB}}^{\text{AiF}}(i+1)$  are further concatenated as  $f_{\text{Con}}^{\text{AiF}}(i)$ , where  $i$  ( $i \in \{2, 3\}$ ) denotes the  $i$ th decoding stage corresponding to the  $i$ th ResNet layer.

2) *Mutual Attention*: Continually taking the  $i$ th decoding stage as an example, a similarity matrix ( $Sim_i$ ) between the features from two branches is computed as:

$$Sim_i = F(f_{\text{Con}}^{\text{Dep}}(i))^T \otimes F(f_{\text{Con}}^{\text{AiF}}(i)), \quad (1)$$

where  $F(\cdot)$  represents a flatten operation reshaping the 3D feature matrix  $f_{\text{Con}}^{\text{AiF}}(i) \in \mathbb{R}^{H \times W \times C}$  to a 2D one with a dimension of  $C \times HW$ ,  $\otimes$  denotes matrix multiplication. Inspired by [26], the  $Sim_i$  is then column-/row-wisely normalized via:

$$\begin{aligned} F_{\text{Sim}}^{\text{AiF}}(i) &= \text{Softmax}(Sim_i) \in [0, 1]^{HW \times HW}, \\ F_{\text{Sim}}^{\text{Dep}}(i) &= \text{Softmax}(Sim_i^T) \in [0, 1]^{HW \times HW}, \end{aligned} \quad (2)$$

where  $\text{Softmax}(\cdot)$  normalizes each column of the  $HW \times HW$  matrix. As shown in Fig. 2, the mutual attentions ( $f_{\text{Sim}}^{\text{AiF}}(i)$ ,  $f_{\text{Sim}}^{\text{Dep}}(i)$ ) for each of the branches are computed as:

$$\begin{aligned} f_{\text{Sim}}^{\text{AiF}}(i) &= R(F_{\text{Sim}}^{\text{AiF}}(i) \otimes F(f_{\text{Con}}^{\text{Fus}}(i))^T) \in [0, 1]^{H \times W \times C}, \\ f_{\text{Sim}}^{\text{Dep}}(i) &= R(F_{\text{Sim}}^{\text{Dep}}(i) \otimes F(f_{\text{Con}}^{\text{Fus}}(i))^T) \in [0, 1]^{H \times W \times C}, \end{aligned} \quad (3)$$

where  $R(\cdot)$  reshapes the given matrix from a dimension of  $C \times HW$  to  $H \times W \times C$ ,  $F(f_{\text{Con}}^{\text{Fus}}(i))$  denotes fused features from both branches (Fig. 2), which is the main difference when compared to [27]. To further avoid unstable feature updating during the model training process, a pair of self-adapted gate functions ( $G_i^{\text{AiF}}$ ,  $G_i^{\text{Dep}}$ ) are computed to gain the final mutual attention matrix ( $f_{\text{MA}}^{\text{AiF}}(i)$ ,  $f_{\text{MA}}^{\text{Dep}}(i)$ ). The process can be described as:

$$f_{\text{MA}}^{\text{AiF}}(i) = G_i^{\text{AiF}} \odot f_{\text{Sim}}^{\text{AiF}}(i) \text{ and } f_{\text{MA}}^{\text{Dep}}(i) = G_i^{\text{Dep}} \odot f_{\text{Sim}}^{\text{Dep}}(i), \quad (4)$$

where  $\odot$  represents Hadamard product, the gate function  $G_i^{\text{AiF}} = \sigma(\text{Conv}(f_{\text{Sim}}^{\text{AiF}}(i)))$  with  $\text{Conv}(\cdot)$  and  $\sigma(\cdot)$  denoting a convolutional layer and a Sigmoid function, respectively. In *CMA-Net*, we cascade two identical mutual attention modules to establish the decoder, thus acquiring the best performance (see detailed ablation studies in § IV-C).

### C. Co-Supervision and Hybrid Loss

As shown in Fig. 2, to stabilize the multi-modal learning process, we apply a three-way strategy to co-supervise the training of our *CMA-Net*. Besides, inspired by a multi-loss function training setting applied in [28], we combine three loss functions including widely used binary cross entropy loss ( $\ell_{\text{BCE}}$ ), intersection over union loss ( $\ell_{\text{IoU}}$ ) and E-loss ( $\ell_{\text{EM}} = 1 - E_\phi$ ), which is based on a recently proposed SOD metric ( $E_\phi$  [29]). Therefore, our hybrid loss function is denoted as:

$$\ell = \sum_{n=1}^N \ell_{\text{BCE}}(P_n, G) + \ell_{\text{IoU}}(P_n, G) + \ell_{\text{EM}}(P_n, G), \quad (5)$$

where  $\{P_n\}_{n=1}^3 \in [0, 1]$  denote the predicted three-way saliency maps, while  $G \in \{0, 1\}$  denotes the corresponding ground-truth binary mask.

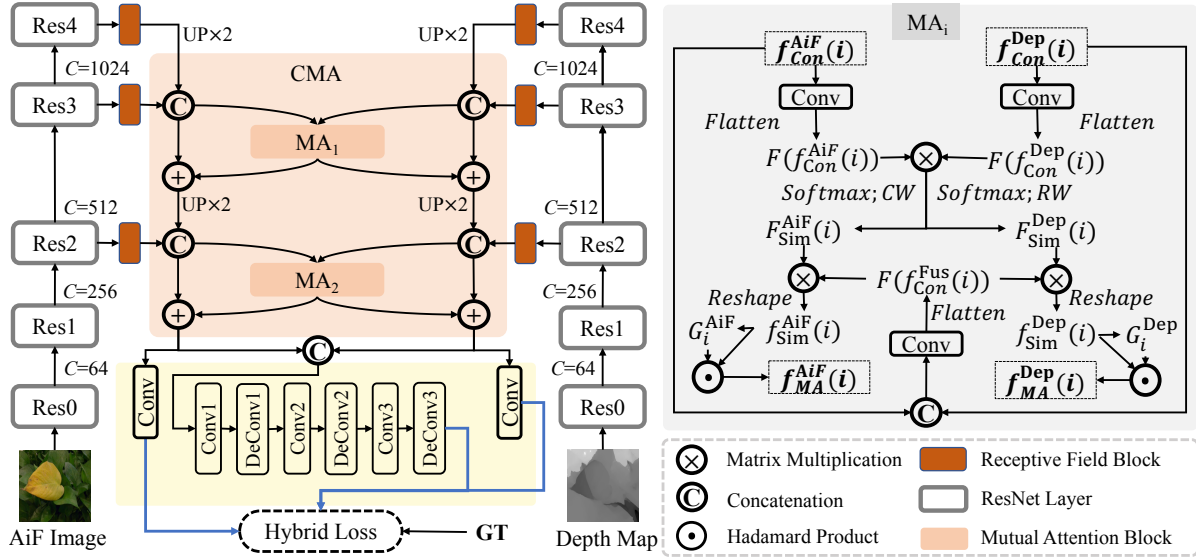


Fig. 2. An overview of our *CMA-Net*. RGB-D high level features extracted from dual-branch encoder are fed into two proposed cascaded mutual attention modules, followed by a group of (de-)convolutional layers from [10]. The abbreviations in the figure are detailed as follows: AiF Image = all-in-focus image. GT = ground truth. Res $i$  = the  $i$ th ResNet [24] layer. (De)Conv = (de-)convolutional layer. MA $_i$  = the  $i$ th mutual attention module. CMA = cascaded mutual attention module. CW = column-wise normalization. RW = row-wise normalization.

#### D. Implementation Details

Our *CMA-Net* is implemented in PyTorch 1.8 and optimized with Adam algorithm [30]. During the training stage, the batch size is set to 16, the learning rate is initialized as  $1e-4$  with a decay rate of 0.1 for every 50 epochs. It takes about one hour to finish the training of *CMA-Net* based on a platform consists of Intel<sup>®</sup> Xeon(R) W-2255 CPU @ 3.70GHz and one Quadro RTX 6000 GPU.

### IV. EXPERIMENTS

#### A. Datasets and Evaluations

We evaluate our *CMA-Net* and 30 baselines on two widely used light field SOD datasets, i.e., DUT-LF [7] and HFUT [6] (more description in § II-A). We follow the training/testing settings in [9], which is so far the largest light field SOD benchmark.

To quantitatively compare our *CMA-Net* with the others, we apply four widely applied SOD metrics, including recently proposed S-measure ( $S_\alpha$ ) [51] and E-measure ( $E_\phi$ ) [29], generally agreed mean absolute error ( $M$ ) [52] and F-measure ( $F_\beta$ ) [53]. Specifically,  $S_\alpha$  evaluates the structure similarities between salient objects in ground-truth maps and predicted saliency maps:

$$S_\alpha = \alpha \times S_o + (1 - \alpha) \times S_r. \quad (6)$$

where  $S_o$  and  $S_r$  denotes the object-/region-based structure similarities, respectively.  $\alpha \in [0, 1]$  is set as 0.5 so that equal weights are assigned to both the object-level and region-level assessments [51].  $E_\phi$  is a cognitive vision-inspired metric to

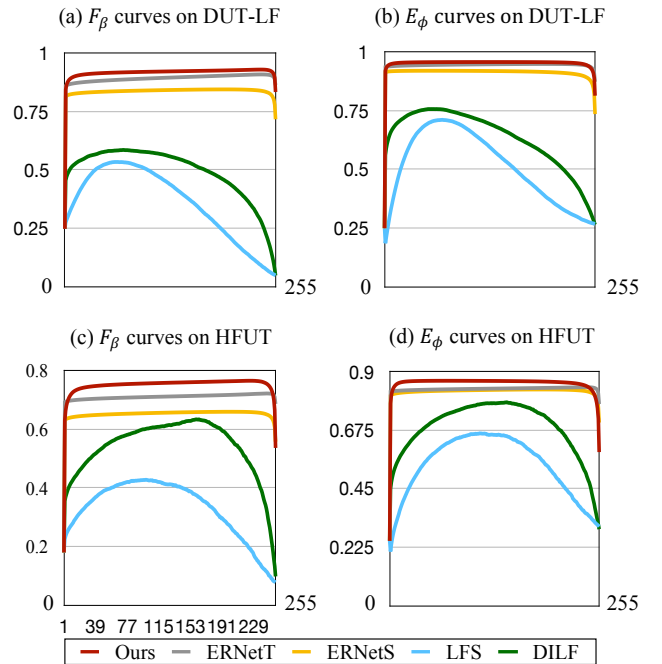


Fig. 3. F-measure ( $F_\beta$ ) and E-measure ( $E_\phi$ ) curves of state-of-the-art light field SOD models and our *CMA-Net* upon two benchmark datasets.

evaluate both the local and global similarities between two binary maps. It is defined as:

$$E_\phi = \frac{1}{W \times H} \sum_{x=1}^W \sum_{y=1}^H \phi(P(x, y), G(x, y)), \quad (7)$$

where  $\phi$  represents the enhanced alignment matrix [29],  $H$  and  $W$  denotes height and width, respectively.  $M$  computes

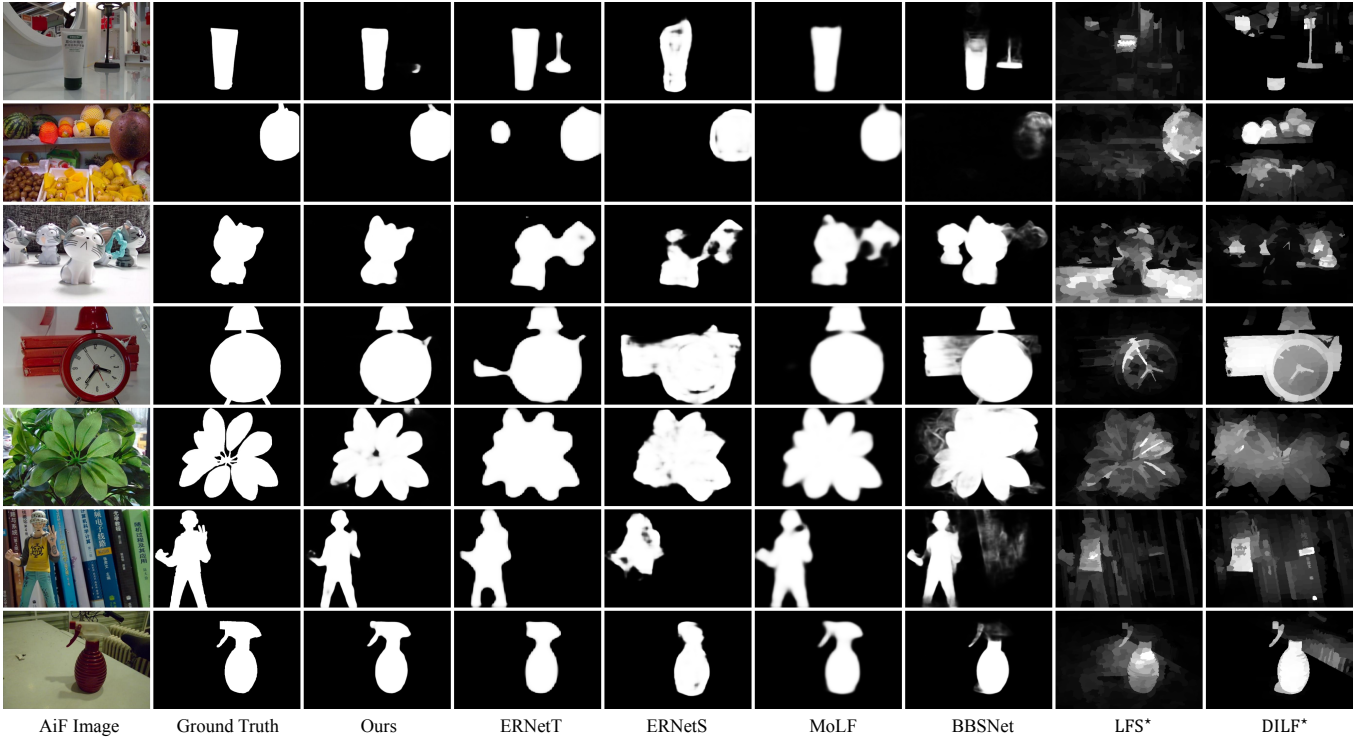


Fig. 4. Visual results our *CMA-Net* and state-of-the-art multi-modal SOD models.  $\star$  denotes traditional methods. AiF Image = all-in-focus image.

the mean absolute error between the ground truth  $G \in \{0, 1\}$  and a normalized predicted saliency map  $P \in [0, 1]$ , i.e.,

$$M = \frac{1}{W \times H} \sum_{i=1}^W \sum_{j=1}^H |G(i, j) - P(i, j)|, \quad (8)$$

$F_\beta$  gives a single-valued metric by considering both the *Precision* and *Recall*:

$$F_\beta = \frac{(1 + \beta^2) \text{Precision} \times \text{Recall}}{\beta^2 \text{Precision} + \text{Recall}}, \quad (9)$$

with

$$\text{Precision} = \frac{|F \cap G|}{|F|}; \text{Recall} = \frac{|F \cap G|}{|G|}, \quad (10)$$

where  $F$  denotes a binary mask converted from a predicted saliency map and  $G$  is the ground truth. Multiple  $F$  are computed by taking different thresholds of  $[0, 255]$  on the predicted saliency map. The  $\beta^2$  is set to 0.3 according to [53]. In this paper, we report adaptive  $F_\beta/E_\phi$ , thus being consistent with ERNetT [9] and MoLF [4].

### B. Comparison with the State-of-the-Arts

1) *Quantitative Results*: As shown in Tab. I, our *CMA-Net* outperforms 30 state-of-the-art methods on all four metrics. Besides, as shown in Fig. 3, our *CMA-Net* is also able to acquire the best performance on each threshold ( $\tau, \tau \in [0, 255]$ ) of F/E-measure curves. The sufficient quantitative results indicate the effectiveness as well as robustness of the proposed *CMA-Net*.

2) *Qualitative Results*: Some visual results of our *CMA-Net* and six advanced baselines are shown in Fig. 4. The *CMA-Net* predicts saliency maps that are closest to the ground-truth, by finely depicting the shapes and boundaries of the labeled salient objects.

3) *Inference Speed*: It is worth mentioning that our *CMA-Net* is capable of running at 53 fps, being much more efficient than the top-ranked ERNetT [9] which owns an inference speed of only 14 fps.

### C. Ablation Studies

We conduct thorough ablation studies to further verify the effectiveness of each module of the proposed method. We first construct basic model-1 which consists of single-branch ResNet layers and a group of (de-)convolutional layers, without the inputs of depth maps. Followed by model-2, which contains the duel-branch encoder with both AiF images and depth maps as inputs. As a result, we find that depth information can be helpful for the SOD task (Tab. II). We then carefully add mutual attention mechanisms to different decoding stages. The model-3 and model-4 are embedded with one mutual attention module at the  $2^{nd}$  and  $3^{rd}$  stages (§ III), respectively. Finally, we cascade two mutual attention modules (*CMA-Net*) and thus gaining the best performance compared to all ablated versions (Tab. II).

## V. CONCLUSION

In this paper, we conduct light field SOD by proposing a new deep learning method, *CMA-Net*, which consists of two cascaded novel mutual attention modules for RGB-D

TABLE I

QUANTITATIVE RESULTS FOR DIFFERENT MODELS ON TWO BENCHMARK DATASETS. THE BEST SCORES ARE IN **BOLDFACE**. WE TRAIN AND TEST OUR *CMA-Net* WITH THE SETTINGS THAT ARE CONSISTENT WITH [9], WHICH IS THE STATE-OF-THE-ART MODEL AT PRESENT. \* INDICATES TRADITION METHODS.  $\uparrow$  INDICATES THE HIGHER THE SCORE THE BETTER, AND VICE VERSA FOR  $\downarrow$ .

Models	DUT-LF [7]				HFUT [6]			
	$F_\beta \uparrow$	$S_\alpha \uparrow$	$E_\phi \uparrow$	$M \downarrow$	$F_\beta \uparrow$	$S_\alpha \uparrow$	$E_\phi \uparrow$	$M \downarrow$
Ours	<b>0.917</b>	<b>0.918</b>	<b>0.949</b>	<b>0.033</b>	<b>0.744</b>	<b>0.807</b>	<b>0.865</b>	<b>0.069</b>
ERNetT [9]	0.889	0.899	0.943	0.040	0.705	0.777	0.831	0.082
ERNetS [9]	0.838	0.848	0.916	0.061	0.651	0.736	0.824	0.085
MoLF [4]	0.843	0.887	0.923	0.052	0.627	0.742	0.785	0.095
DLFS [8]	0.801	0.841	0.891	0.076	0.615	0.741	0.783	0.098
DILF* [18]	0.641	0.705	0.805	0.168	0.555	0.695	0.736	0.131
LFS* [5]	0.484	0.563	0.728	0.240	0.430	0.579	0.686	0.205
BBSNet [10]	0.854	0.865	0.908	0.066	0.705	0.783	0.829	0.078
UCNet [31]	0.817	0.831	0.878	0.081	0.710	0.770	0.830	0.084
S2MA [22]	0.754	0.787	0.841	0.103	0.647	0.761	0.787	0.100
D3Net [32]	0.790	0.822	0.869	0.084	0.692	0.778	0.827	0.080
CPFP [33]	0.730	0.741	0.808	0.101	0.594	0.701	0.768	0.096
TANet [34]	0.771	0.803	0.861	0.096	0.638	0.744	0.789	0.096
MMCI [35]	0.750	0.785	0.853	0.116	0.645	0.741	0.787	0.104
PDNet [36]	0.763	0.803	0.864	0.111	0.629	0.770	0.786	0.105
PCA [37]	0.762	0.800	0.857	0.100	0.644	0.748	0.782	0.095
CTMF [38]	0.790	0.823	0.881	0.100	0.620	0.752	0.784	0.103
DF [39]	0.733	0.716	0.838	0.151	0.562	0.670	0.742	0.138
F3Net [28]	0.882	0.888	0.900	0.057	0.718	0.777	0.815	0.095
GCPANet [40]	0.867	0.885	0.898	0.064	0.691	0.777	0.799	0.105
EGNet [41]	0.870	0.886	0.914	0.053	0.672	0.772	0.794	0.094
CPD [25]	0.887	0.890	0.923	0.050	0.689	0.764	0.810	0.097
PoolNet [42]	0.868	0.889	0.919	0.051	0.683	0.776	0.802	0.092
PAGRN [43]	0.828	0.822	0.878	0.084	0.635	0.717	0.773	0.114
C2S [44]	0.791	0.844	0.874	0.084	0.650	0.763	0.786	0.111
R <sup>3</sup> Net [45]	0.783	0.819	0.833	0.113	0.625	0.727	0.728	0.151
Amulet [46]	0.805	0.847	0.882	0.083	0.636	0.767	0.760	0.110
UCF [47]	0.769	0.837	0.850	0.107	0.623	0.754	0.764	0.130
SRM [48]	0.832	0.848	0.899	0.072	0.672	0.762	0.801	0.096
NLDF [49]	0.778	0.786	0.862	0.103	0.636	0.729	0.807	0.091
DSS [50]	0.728	0.764	0.827	0.128	0.626	0.715	0.778	0.133

cross modal high-level feature fusion. Our *CMA-Net* achieves the best performance on widely used light field benchmark datasets based on four commonly agreed SOD metrics, also with a competing inference speed of 53 fps. Systematical ablation studies are also conducted to verify the effectiveness of the proposed attention mechanism as well as the feasibility of RGB-D cross modal learning strategy for light field SOD.

## REFERENCES

[1] F. Perazzi, J. Pont-Tuset, B. McWilliams, L. Van Gool, M. Gross, and A. Sorkine-Hornung, "A benchmark dataset and evaluation methodology for video object segmentation," in *IEEE CVPR*, pp. 724–732, 2016.

TABLE II

QUANTITATIVE RESULTS FOR THE ABLATION STUDIES OF *CMA-Net* ON DUT-LF [7] AND HFUT [6]. THE BEST SCORES ARE IN **BOLDFACE**.  $\uparrow$  INDICATES THE HIGHER THE SCORE THE BETTER, AND VICE VERSA FOR  $\downarrow$ .

Metric	Model-1	Model-2	Model-3	Model-4	<i>CMA-Net</i>	
DUT-LF	$F_\beta \uparrow$	0.879	0.895	0.914	0.915	<b>0.917</b>
	$S_\alpha \uparrow$	0.893	0.911	0.916	0.916	<b>0.918</b>
	$E_\phi \uparrow$	0.931	0.943	0.949	<b>0.950</b>	0.949
	$M \downarrow$	0.047	0.039	0.034	0.034	<b>0.033</b>
HFUT	$F_\beta \uparrow$	0.697	0.704	0.727	0.729	<b>0.744</b>
	$S_\alpha \uparrow$	0.792	0.795	0.791	0.791	<b>0.807</b>
	$E_\phi \uparrow$	0.837	0.828	0.842	0.858	<b>0.865</b>
	$M \downarrow$	0.074	0.078	0.076	0.071	<b>0.069</b>

[2] L. Zhang, J. Zhang, Z. Lin, H. Lu, and Y. He, "Capsal: Leveraging captioning to boost semantics for salient object detection," in *IEEE CVPR*, pp. 6024–6033, 2019.

[3] Y. Zhang, L. Zhang, W. Hamidouche, and O. Deforges, "Key issues for the construction of salient object datasets with large-scale annotation," in *IEEE MIPR*, pp. 117–122, 2020.

[4] M. Zhang, J. Li, J. Wei, Y. Piao, and H. Lu, "Memory-oriented decoder for light field salient object detection," in *NeurIPS*, 2019.

[5] N. Li, J. Ye, Y. Ji, H. Ling, and J. Yu, "Saliency detection on light field," in *CVPR*, 2014.

[6] J. Zhang, M. Wang, L. Lin, X. Yang, J. Gao, and Y. Rui, "Saliency detection on light field: A multi-cue approach," *TOMM*, 2017.

[7] T. Wang, Y. Piao, H. Lu, X. chun Li, and L. Zhang, "Deep learning for light field saliency detection," in *ICCV*, 2019.

[8] Y. Piao, Z. Rong, M. Zhang, X. Li, and H. Lu, "Deep light-field-driven saliency detection from a single view," in *IJCAI*, 2019.

[9] Y. Piao, Z. Rong, M. Zhang, and H. Lu, "Exploit and replace: an asymmetrical two-stream architecture for versatile light field saliency detection," in *AAAI*, 2020.

[10] D.-P. Fan, Y. Zhai, A. Borji, J. Yang, and L. Shao, "Bbs-net: Rgb-d salient object detection with a bifurcated backbone strategy network," in *ECCV*, 2020.

[11] N. Li, B. Sun, and J. Yu, "A weighted sparse coding framework for saliency detection," in *CVPR*, 2015.

[12] H. Sheng, S. Zhang, X. Liu, and Z. Xiong, "Relative location for light field saliency detection," in *ICASSP*, 2016.

[13] A. Wang, M. Wang, X. Li, Z. Mi, and H. Zhou, "A two-stage bayesian integration framework for salient object detection on light field," *Neural Processing Letters*, 2017.

[14] H. Wang, B. Yan, X. Wang, Y. Zhang, and Y. Yang, "Accurate saliency detection based on depth feature of 3d images," *Multimedia Tools and Applications*, 2018.

[15] S. Wang, W. Liao, P. Surman, Z. Tu, Y. Zheng, and J. Yuan, "Saliency guided depth calibration for perceptually optimized compressive light field 3d display," in *CVPR*, 2018.

[16] X. Wang, Y. Dong, Q. Zhang, and Q. Wang, "Region-based depth feature descriptor for saliency detection on light field," *Multimedia Tools and Applications*, 2020.

[17] Y. Piao, X. Li, M. Zhang, J. Yu, and H. Lu, "Saliency detection via depth-induced cellular automata on light field," *TIP*, 2020.

[18] J. Zhang, M. Wang, J. Gao, Y. Wang, X. Zhang, and X. Wu, "Saliency detection with a deeper investigation of light field," in *IJCAI*, 2015.

[19] M. Zhang, W. Ji, Y. Piao, J. Li, Y. Zhang, S. Xu, and H. Lu, "Lfnnet: Light field fusion network for salient object detection," *TIP*, 2020.

[20] J. Zhang, Y. Liu, S. Zhang, R. Poppe, and M. Wang, "Light field saliency detection with deep convolutional networks," *TIP*, 2020.

[21] Q. Zhang, S. Wang, X. Wang, Z. Sun, S. Kwong, and J. Jiang, "A multi-task collaborative network for light field salient object detection," *TCSVT*, 2020.

[22] N. Liu, N. Zhang, and J. Han, "Learning selective self-mutual attention for rgb-d saliency detection," in *CVPR*, 2020.

[23] J. Hu, L. Shen, and G. Sun, "Squeeze-and-excitation networks," in *CVPR*, 2018.

- [24] K. He, X. Zhang, S. Ren, and J. Sun, "Deep residual learning for image recognition," in *CVPR*, 2016.
- [25] Z. Wu, L. Su, and Q. Huang, "Cascaded partial decoder for fast and accurate salient object detection," in *CVPR*, 2019.
- [26] X. Lu, W. Wang, J. Shen, D. Crandall, and J. Luo, "Zero-shot video object segmentation with co-attention siamese networks," *TPAMI*, 2020.
- [27] Y. Zhang, G. Chen, Q. Chen, Y. Sun, O. Deforges, and L. Zhang, "Learning synergistic attention for light field salient object detection," *arXiv preprint arXiv:2104.13916*, 2021.
- [28] J. Wei, S. Wang, and Q. Huang, "F<sup>3</sup>net: Fusion, feedback and focus for salient object detection," in *AAAI*, 2020.
- [29] D.-P. Fan, C. Gong, Y. Cao, B. Ren, M.-M. Cheng, and A. Borji, "Enhanced-alignment measure for binary foreground map evaluation," in *IJCAI*, 2018.
- [30] D. P. Kingma and J. Ba, "Adam: A method for stochastic optimization," in *ICLR*, 2015.
- [31] J. Zhang, D.-P. Fan, Y. Dai, S. Anwar, F. S. Saleh, T. Zhang, and N. Barnes, "Uc-net: uncertainty inspired rgb-d saliency detection via conditional variational autoencoders," in *ICCV*, 2020.
- [32] D.-P. Fan, Z. Lin, Z. Zhang, M. Zhu, and M.-M. Cheng, "Rethinking rgb-d salient object detection: Models, data sets, and large-scale benchmarks," *TNNLS*, 2020.
- [33] J.-X. Zhao, Y. Cao, D.-P. Fan, M.-M. Cheng, X.-Y. Li, and L. Zhang, "Contrast prior and fluid pyramid integration for rgb-d salient object detection," in *CVPR*, 2019.
- [34] H. Chen and Y. Li, "Three-stream attention-aware network for RGB-D salient object detection," *TIP*, 2019.
- [35] H. Chen, Y. Li, and D. Su, "Multi-modal fusion network with multi-scale multi-path and cross-modal interactions for RGB-D salient object detection," *Pattern Recognition*, 2019.
- [36] C. Zhu, X. Cai, K. Huang, T. H. Li, and G. Li, "PDNet: Prior-model guided depth-enhanced network for salient object detection," in *ICME*, 2019.
- [37] H. Chen and Y. Li, "Progressively complementarity-aware fusion network for rgb-d salient object detection," in *CVPR*, 2018.
- [38] J. Han, H. Chen, N. Liu, C. Yan, and X. Li, "CNNs-based RGB-D saliency detection via cross-view transfer and multiview fusion," *IEEE Transactions on Cybernetics*, 2017.
- [39] L. Qu, S. He, J. Zhang, J. Tian, Y. Tang, and Q. Yang, "Rgbd salient object detection via deep fusion," *TIP*, 2017.
- [40] C. Zuyao, X. Qianqian, C. Runmin, and H. Qingming, "Global context-aware progressive aggregation network for salient object detection," in *AAAI*, 2020.
- [41] J.-X. Zhao, J.-J. Liu, D.-P. Fan, Y. Cao, J. Yang, and M.-M. Cheng, "Egnet: Edge guidance network for salient object detection," in *ICCV*, 2019.
- [42] J.-J. Liu, Q. Hou, M.-M. Cheng, J. Feng, and J. Jiang, "A simple pooling-based design for real-time salient object detection," in *ICCV*, 2019.
- [43] X. Zhang, T. Wang, J. Qi, H. Lu, and G. Wang, "Progressive attention guided recurrent network for salient object detection," in *CVPR*, 2018.
- [44] X. Li, F. Yang, H. Cheng, W. Liu, and D. Shen, "Contour knowledge transfer for salient object detection," in *ECCV*, 2018.
- [45] Z. Deng, X. Hu, L. Zhu, X. Xu, J. Qin, G. Han, and P.-A. Heng, "R3net: Recurrent residual refinement network for saliency detection," in *IJCAI*, 2018.
- [46] P. Zhang, D. Wang, H. Lu, H. Wang, and X. Ruan, "Amulet: Aggregating multi-level convolutional features for salient object detection," in *ICCV*, 2017.
- [47] P. Zhang, D. Wang, H. Lu, H. Wang, and B. Yin, "Learning uncertain convolutional features for accurate saliency detection," in *ICCV*, 2017.
- [48] T. Wang, A. Borji, L. Zhang, P. Zhang, and H. Lu, "A stagewise refinement model for detecting salient objects in images," in *ICCV*, 2017.
- [49] Z. Luo, A. Mishra, A. Achkar, J. Eichel, S. Li, and P.-M. Jodoin, "Non-local deep features for salient object detection," in *CVPR*, 2017.
- [50] Q. Hou, M.-M. Cheng, X. Hu, A. Borji, Z. Tu, and P. H. Torr, "Deeply supervised salient object detection with short connections," in *CVPR*, 2017.
- [51] D.-P. Fan, M.-M. Cheng, Y. Liu, T. Li, and A. Borji, "Structure-measure: A new way to evaluate foreground maps," in *ICCV*, 2017.
- [52] F. Perazzi, P. Krähenbühl, Y. Pritch, and A. Hornung, "Saliency filters: Contrast based filtering for salient region detection," in *CVPR*, 2012.
- [53] R. Achanta, S. Hemami, F. Estrada, and S. Susstrunk, "Frequency-tuned salient region detection," in *CVPR*, 2009.